LA-UR-16-23718 (Accepted Manuscript)

A test of the significance of intermolecular vibrational coupling in isotopic fractionation

Herman, Michael F.
Currier, Robert Patrick
Peery, Travis B.
Clegg, Samuel M.

To be published in: Chemical Physics

DOI to publisher's version: 10.1016/j.chemphys.2017.06.005

Permalink to record: http://permalink.lanl.gov/object/view?what=info:lanl-repo/lareport/LA-UR-16-23718

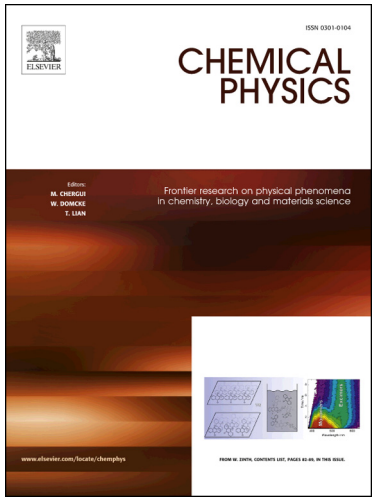

A Test of the Significance of Intermolecular Vibrational Coupling in Isotopic Fractionation

Michael F. Herman, Robert P. Currier, Travis B. Peery, Samuel M. Clegg

PII: S0301-0104(17)30085-X
DOI: http://dx.doi.org/10.1016/j.chemphys.2017.06.005
Reference: CHEMPH 9809

To appear in: *Chemical Physics*

Received Date: 3 February 2017
Revised Date: 1 May 2017
Accepted Date: 12 June 2017

Please cite this article as: M.F. Herman, R.P. Currier, T.B. Peery, S.M. Clegg, A Test of the Significance of Intermolecular Vibrational Coupling in Isotopic Fractionation, *Chemical Physics* (2017), doi: http://dx.doi.org/10.1016/j.chemphys.2017.06.005

A Test of the Significance of Intermolecular Vibrational Coupling in Isotopic Fractionation

Michael F. Herman,[a] Robert P. Currier,[b] Travis B. Peery,[b] and Samuel M. Clegg[b]

[a]Department of Chemistry, Tulane University, New Orleans, LA 70118 USA

[b]Los Alamos National Laboratory, P.O. Box 1663, Los Alamos, NM 87545 USA

Acknowledgements

MFH thanks both the Chemistry and Applied Engineering and Technology Divisions for their hospitality during his visit at Los Alamos National Laboratory. SMC and RPC gratefully acknowledge support from the National Nuclear Security Administration Office of Defense Nuclear Nonproliferation Research and Development and the US National Energy Technology Laboratory's Carbon Capture, Use, and Sequestration Program. Their work was supported under DOE contract number DE-AC52-06NA25396.

Abstract

Intermolecular coupling of dipole moments is studied for a model system consisting of two diatomic molecules (AB monomers) arranged co-linearly and which can form non-covalently bound dimers. The dipolar coupling is a function of the bond length in each molecule as well as of the distance between the centers-of-mass of the two molecules. The calculations show that intermolecular coupling of the vibrations results in an isotope-dependent modification of the AB-AB intermolecular potential. This in turn alters the energies of the low-lying bound states of the dimers, producing isotope-dependent changes in the AB-AB dimer partition function. Explicit inclusion of intermolecular vibrational coupling then changes the predicted gas-dimer isotopic fractionation. In addition, a mass dependence in the intermolecular potential can also result in

changes in the number of bound dimer states in an equilibrium mixture. This in turn leads to a significant dimer population shift in the model monomer-dimer equilibrium system considered here. The results suggest that intermolecular coupling terms should be considered when probing the origins of isotopic fractionation.

Keywords: isotopic fractionation, intermolecular vibrational coupling

I. Introduction

Isotopologues of a molecule differ in the isotope present in one or more of the atoms comprising the molecule. The isotopic composition in a given sample is known to depend on how the constituent molecules were formed and the phase equilibria they underwent. Sample-to-sample variations in isotopic composition are typically a few tenths of 1% and are usually reported as pars per mil (i.e. part per thousand). However, these small deviations can provide important information regarding the processes and conditions that led to the formation of the molecules in a given sample.

Early treatments of isotopologue thermodynamics focused largely on the direct effect of mass differences and differences in zero-point energies[1-5]. Such conventional prescriptions predict, for example, that the vapor phase should always be enriched in the lighter isotopologue when in equilibrium with a condensed phase. In addition, the chemical bonds in a molecule will require more energy to break in a heavier isotopologue due to its lower zero-point vibrational energy. As a result, the activation energy for a reaction will be higher and the reaction slower for the heavier isotopologue using conventional approaches.

However, there are many experimental cases in which these conventional predictions are incomplete, indicating that other physical aspects can play an important role. For instance, there are examples of vapor-liquid and vapor-solid phase equilibria in which the vapor is enriched in

the heavier isotopologue[5-14]. In some chemical processes, such as the extraction of certain metals with crown ethers, fractionation appears to depend significantly on whether the nuclear mass number of the metal atom is even or odd[15-19]. Some chemical reactions also do not obey predictions based solely on zero-point energy considerations, where the heavier species reportedly show faster rather than slower kinetics[20]. Furthermore, the formation of O_3 seems to be largely independent of the isotopic composition of the reactants[21-25], and similar results have also been observed in other reactions.[26-30]. Proposed explanations of these observations include changes in the size and spin of the nucleus[31-33] as well as variations in transition state electronic structure[25,34]. Also, in gas chromatography, it has been observed that heavier isotopologues of carbon dioxide can elude from the column before lighter CO_2 isotopologues.[35]

It has recently been pointed out that dipole moment variation accompanying changes in the internal coordinates of a molecule results in a coupling of the vibrational modes of the different molecules[36]. *This leads to a dependence of the intermolecular forces on the isotopic composition of the molecules.* In this paper, the significance of this mass dependence arising from the vibrational and Lennard-Jones interactions is investigated quantitatively using a simple 1-D model system consisting of collinear interacting diatomic monomer molecules. The goal is to utilize this model to provide insight into the question of whether inclusion of the intermolecular coupling between different isotopologue vibrations can have a significant effect on the thermodynamic properties of an isotopologue mixture. In our model system, two AB molecules align co-linearly in an AB-AB arrangement, so that the dipole-dipole interaction is attractive, and we also consider the AB-BA and BA-AB configurations in which the dipole-dipole interaction is repulsive. The Lennard-Jones(LJ) interactions employed in this work are strong enough that the attractive interactions support non-covalent bound dimer states in all three configurations. This model is similar in spirit to the one-dimensional model employed by Balan

et al. to investigate the isotope dependence of sulfur gas absorption on a surface[37]. In our calculations, isotopic masses and parameters defining the potential energy of the system are taken from the NO molecule, since this is a diatomic molecule with a moderate dipole moment of about 0.16 Debye with a known bond length dependence[38]. The goal of this work is *not* to provide a complete theoretical description of any specific AB-AB dimer, since a complete description would also depend on features not included in this simple model, such as, the rotations of the molecules and the three-dimensional motion of the vector between centers of mass of the two molecules. Furthermore, the isotopic fractionation in a real system would also have to account for any reactions involving covalent bonding. For instance, the real NO molecule has an unpaired electron and can form a covalent bond between the N atoms of the two NO molecules[39]. Since dimers are bound in this model due to the Lennard-Jones interactions, they are an example (within a simplified model) of a van der Waals complex[40-42].

Conventional Monte Carlo and molecular dynamics simulations are often performed using force fields to model the interactions between the different atoms, or groups of atoms, in each of the molecules. Such simulations generally do not account for the bond length dependence of the coupling of the vibrations of different molecules. Thus, the question of the thermodynamic significance of the mass-dependent intermolecular coupling is an important one. Hou *et al.* have recently reported calculations which demonstrate that inclusion of the dependence of the H_2O-Ar potential energy surface on the *intramolecular* coupling of the vibrational modes of H_2O is necessary to obtain a high level of accuracy[43]. This work, on the other hand, focuses on *intermolecular* vibrational couplings. It should also be noted that several computational studies on the quantum nature of hydrogen isotopes in water and in hydrogen shift reactions have been performed using quantum path integral techniques[44-48]. The less computationally demanding method presented here would not, in its current form, account for

the light nuclei quantum effects considered in those studies. The quantum path integral calculations would also account for the isotope mass dependence for the interactions between the molecules that is considered in this work, as would higher-level quantum chemistry methods. However, force fields are still useful for large systems, and it is important to note that obtaining the correct isotope fractionation requires that these bond length dependent intermolecular interactions be included.

The organization of this paper is as follows. The one dimensional, co-linear two AB model is described in section II.A. The semiclassical method used for evaluating the two AB bound state energies is presented in section II. B. Results are presented in section II.C, which show that mass dependent intermolecular vibrational couplings can have an important effect on isotopic fractionation in the non-covalent monomer-dimer reaction, and the mass dependent interaction also results in changes in the fraction of AB present in dimer form. These results and their potential importance in more complicated molecular systems are discussed in section III.

II. Calculations

A. AB Dimer Model

The model employed in this work consists of two AB molecules (denoted as 1 and 2) with all four atoms aligned co-linearly, as shown in fig. 1 for an AB_1-AB_2 alignment. The separation between the centers-of-mass (COM) of the two molecules is denoted as R and the bond lengths for the two molecules are r_1 and r_2. The model potential energy for this alignment then has the following form:

$$V(R, r_1, r_2) = V_M(r_1) + V_M(r_2) + V_{AA}(R + a_1r_1 - a_2r_2) + V_{BB}(R - b_1r_1 + b_2r_2) + \\ + V_{AB}(R + a_1r_1 + b_2r_2) + V_{AB}(R - b_1r_1 - a_2r_2) + V_\mu(R, r_1, r_2) \qquad (1)$$

where $a_j r_j$ and $b_j r_j$ are the distances of the A and B atoms, respectively, from the COM of molecule j (j = 1 or 2),

$$V_M(r) = D(1 - \exp[-\alpha(r - r_e)])^2 \quad (2)$$

is the Morse potential employed to model the bond length dependence of the energy of a AB molecule,

$$V_{IJ}(r) = 4\varepsilon_{IJ}[(\sigma_{IJ}/r)^{12} - (\sigma_{IJ}/r)^6] \quad (3)$$

(with IJ = AA, BB, or AB) is the Lennard-Jones (LJ) interaction between atoms I and J separated by the distance r, and

$$V_\mu(R, r_1, r_2) = - 2\mu(r_1)\mu(r_2)/R^3 \quad (4)$$

is the dipole-dipole interaction between the two molecules. The dipoles are taken to have a bond length dependence of the form

$$\mu(r) = \mu_0 + \mu_1(r - r_e) + \mu_2(r - r_e)^2 . \quad (5)$$

The potential energy for the AB-BA and BA-AB case are obtained by changing the sign in Eq. (4) and the appropriate modification of the signs before a_1, a_2, b_1, and b_2 in the LJ terms in Eq.(1).

The LJ parameters ε_{AA}, ε_{BB}, σ_{AA}, and σ_{BB} employed here are literature values for N and O obtained from fits to experimental data[49,50]. The LJ parameters for the interaction between an A atom and a B atom are obtained using the combining rules $\varepsilon_{AB} = (\varepsilon_{AA}\varepsilon_{BB})^{1/2}$ and $\sigma_{AB} = (\sigma_{AA} + \sigma_B)/2$. The Morse potential D and α parameters were fit to match experimental values of the NO vibrational constants ω_e and $x_e\omega_e$, while r_e is taken to be the experimental bond length for an isolated NO molecule[51], and the same r_e is used for all isotopologues. The dipole moment of the AB molecule is assumed to have a quadratic dependence on bond length, Eq. (5), where μ_0, μ_1, and μ_2 have values obtained from an analysis of Einstein coefficients for the NO vibrational-rotational transitions[38].

Two types of calculations are reported in this work. In one type, the values of r_1 and r_2 that minimize the potential $V(R, r_1, r_2)$ are found for each value of R, and the power series expansion of $V(R, r_1, r_2)$ in terms of $r_1 - r_{1,min}$ and $r_2 - r_{2,min}$ is used to calculate the (R-dependent) vibrational modes and energies of this coupled two oscillator system. These calculations are referred to as the "coupled" calculations. Calculations are also reported for which the values of r_1 and r_2 are held at r_e when evaluating the Lennard-Jones and dipolar potentials, and the vibrations are taken to be the uncoupled vibrations of the two isolated AB molecules. These are referred to as the "uncoupled" calculations in this work. This parallels the common practice in molecular simulations to evaluate Lennard-Jones and dipolar intermolecular interactions, and the vibrations of the individual molecules are treated as unchanged by the intermolecular interactions, as is the case in the uncoupled calculations reported below.

In coupled calculations, the values of r_1 and r_2 that minimize V for a fixed R are obtained iteratively using the first and second derivatives of V with respect to $\mathbf{r} = (r_1, r_2)$. The R-dependent two dimensional matrix $\partial^2 V / \partial \mathbf{r} \partial \mathbf{r}$ is then evaluated at this minimum, $\mathbf{r}_{min}(R)$, converted to mass-weighted coordinates, and diagonalized to give the force constants k_1 and k_2 for the two vibrational modes. The vibrational frequencies $\omega_1 = \sqrt{k_1}$ and $\omega_2 = \sqrt{k_2}$ are then obtained. These R-dependent force constants also depend on the masses of the two AB molecules through the conversion to mass-weighted coordinates. The third and fourth derivatives of $V(R, r_1, r_2)$ in terms of the mass-weighted vibrational coordinates are also calculated, and these are used in evaluating first and second order perturbation corrections to the vibrational energies. The total energy of the two AB system for the coupled (cpl) calculations is

$$E_{cpl}(R) = V_s(R, \mathbf{r}_{min}) + E_{v,1}(R, \mathbf{r}_{min}) + E_{v,2}(R, \mathbf{r}_{min}) \qquad (6)$$

where $E_{v,j}$ is the ground state energy of vibrational mode j, which is given by

$$E_{v,j}(R,\mathbf{r}_{min}) = E_{0,j}^{(0)}(R,\mathbf{r}_{min}) + E_{0,j}^{(1)}(R,\mathbf{r}_{min}) + E_{0,j}^{(2)}(R,\mathbf{r}_{min}) \quad (7)$$

and the superscripts give the order in perturbation theory[52]. The shifted potential $V_s(R, \mathbf{r})$ in Eq. (6) is $V(R,r_1,r_2) - E_{vib}^{(\infty)}$, where $E_{vib}^{(\infty)}$ is the sum of the ground state vibrational energies in the $R \rightarrow \infty$ limit. With $V_s(R, \mathbf{r})$ defined this way, $E_{cpl}(R) \rightarrow 0$ in the $R \rightarrow \infty$ limit. The $\mathbf{r}_{min}$ in $E_{v,1}(R, \mathbf{r}_{min})$ and $E_{v,2}(R, \mathbf{r}_{min})$ indicates that these vibrational energies are evaluated using an expansion of the potential around $\mathbf{r}_{min}$.

In the uncoupled calculations, the vibrational energy for each molecule is calculated to second order in perturbation theory using an expansion of the Morse potential up to fourth order in $\mathbf{r}$-$\mathbf{r}_e$. This approximation is used for the vibrational energies, rather than the exact Morse ground state energy, since this is the same as the approximation for the vibrational energies in the coupled calculations[52]. The total energy for the AB dimer system in uncoupled (unc) calculations is given by

$$E_{unc}(R) = V_s(R, \mathbf{r}_e) + E_{M,1} + E_{M,2} \quad (8)$$

where $\mathbf{r}_e$ denotes that both r_1 and r_2 are at r_e. Here $E_{M,j}$ is the second order perturbative approximation for the ground state energy of the Morse oscillator using the reduced mass for AB isotopologue j. Note that $V_s(R, \mathbf{r}_e) = V(R, r_e, r_e) - E_{vib}^{(\infty)}$, and $E_{vib}^{(\infty)} = E_{M,1} + E_{M,2}$. As a result, $E_{unc}(R) = V(R, \mathbf{r}_e)$ is just the sum of the LJ and dipolar terms in Eq. (1) with $r_1 = r_2 = r_e$, since the vibrational terms cancel and the Morse potential, $V_M(r)$, is zero at r_e.

B. Evaluation of Dimer Bound State Energies

The energies $E_{cpl}(R)$ and $E_{unc}(R)$ serve as the potential energy for the dynamics of the intermolecular coordinate R for the coupled and uncoupled calculations, respectively. Once $E_{cpl}(R)$ or $E_{unc}(R)$ have been obtained, they are employed to calculate the energies of the AB-AB,

AB-BA, or BA-AB bound states, which in turn are used to evaluate the corresponding dimer partition function. Semiclassical bound states are located at energies for which[53]

$$W(E)/\hbar = (n + 1/2)\pi, \quad (9)$$

where n is an integer, ħ is Planck's constant divided by 2π, and the action W(E) is given by

$$W(E) = \int_{R_{TL}}^{R_{TR}} p(R,E)\,dR \quad (10)$$

In this expression, $p(R, E) = \sqrt{2m_R\left[E - V_d(R)\right]}$ is the momentum for the motion of the R coordinate, and either $E_{cpl}(R)$ or $E_{unc}(R)$ is used for the dimer potential energy, $V_d(R)$. R_{TR} and R_{TL} are the right and left classical turning points for $V_d(R)$ at energy E [i.e. the points at which $V_d(R) = E$] and $m_R = m_1m_2/(m_1 + m_2)$ is the dimer reduced mass with m_1 and m_2 being the masses of the two AB molecules.

Since the momentum is an increasing function of E and the distance between the turning points in Eq. (10) also increases as E increases, W(E) must be an increasing function of E. Furthermore, bound states must have energies less that E = 0, since $V_d(R)$ goes to zero at large R. Therefore, it follows for Eq. (9) that the quantum number of the highest bound state, n_b, is given by the largest integer smaller than $W(0)/\pi\hbar$ - ½. The zero energy action W(0) is calculated by performing the integral in Eq. (10) with E = 0 from the value of R at which $V_d(R) = 0$ to a large value of R. The upper limit of the integration for W(0) should be ∞ for the AB-AB case. At large R, $V_d \sim -R^{-3}$ for the AB-AB alignment, which can be used to obtain an estimate of the error in W(0) when the upper limit is large but at finite R. In these calculations, this error in $W(0)/\hbar$ is on the order of 10^{-3}. It was checked for all calculations that $W(0)/\pi\hbar$ - ½ was further away from an integer value than the truncation error in W(0), showing that the reported values of n_b are accurate.

In the AB-BA and BA-AB cases, $V_\mu \sim R^{-3}$ is greater than zero. As R becomes larger there is a point where V_μ is equal in magnitude to the more rapidly decaying attractive LJ interactions. As R increases past this point, the total potential becomes (very slightly) positive and then decays to zero. The $W(0)/\pi\hbar - ½$ is evaluated for the AB-BA and BA-AB cases by integrating W(0) between the point at which $V_d(R) = 0$ at small R and the point where $V_d(R) = 0$ at large R. For all alignments of the two AB molecule, the energy for each bound state from n = 0 to $n = n_b$ was obtained by an iterative procedure in which a pair of E values were found for which W(E) bracketed the value $(n + 1/2)\pi\hbar$, and then the E_n for which $W(E_n) = (n + 1/2)\pi\hbar$ was obtained iteratively using a locally linear approximation for W(E).

Once the number of dimer bound states, $n_{bnd} = n_b + 1$, and their energies are evaluated, then the partition function for the dimer is given by[54] $q_d = q_b q_{tr,d}$, where q_b is the bound state partition function for the potential $V_d(R)$

$$q_b = \sum_{n=0}^{n_b} e^{-\beta E_n}, \tag{11}$$

and $q_{tr,d}$ is the classical translational partition function for the center of mass of the AB-AB dimer

$$q_{tr,d} = (2\pi M k_B T/h^2)^{1/2}\, V. \tag{12}$$

$M = m_1 + m_2$ is the dimer mass. The volume in the classical translational partition function, V, is just the box length in this one dimensional case. In order to model the thermodynamics of the non-covalent AB dimerization reaction

$$AB_1 + AB_2 \rightarrow AB_1AB_2 \tag{13}$$

the partition function for the two monomer system

$$q_m = q_1 q_{,2} \tag{14}$$

is also needed, where the subscripts 1 and 2 in Eqs. (13) and (14) label the two AB molecules.

The contribution to the vibrational partition functions from excited AB vibrational states is negligible compared to the ground vibrational state contribution, whether it is obtained using the harmonic vibrational frequency of $^{14}N^{16}O$, 1904 cm^{-1} [5] or $^{15}N^{16}O$, or the corresponding ground state frequencies corrected for anharmonicity. Furthermore, the ground state vibrational energies are subtracted from the AB-AB potential, which means the zero of energy corresponds to the separated molecules in their uncoupled vibrational states. Given this zero of energy, the vibrational partition functions for the individual AB molecules are each unity plus a negligible excited state contribution. (The Boltzmann factor corresponding to 1904 cm^{-1} and T = 150 K is about 10^{-8}) Thus, q_1 and q_2 are given by the translational partition function, Eq. (12), with M replaced with m_1 and m_2, respectively.

The error arising from the use of the classical partition function for the free-particle translational motion, Eq. (12) in these calculations, was examined numerically. The partition function in Eq. (12) can be obtained as the large box-length limit of the quantum particle in a box partition function (L = V in Eq. (12)).[55]. The quantum partition function was obtained for the $E > 0$ states using the $V_d(R)$ for the coupled or uncoupled reaction with a hard wall at L (i.e., $V_d = \infty$ if $R \geq L$). (Since there is a hard wall at L, all states are actually "bound" states. However, we will use the bound states here to mean states for which the two AB molecules are held close to each other; i.e., states with $E < 0$. Correspondingly, unbound states refers to states with $E > 0$, since the AB molecules can move far from each other in this case.) The quantum energies were obtained semiclassically in a manner similar to the evaluation of the bound state energies described above.[56] Using $V_d(R)$ in the calculations shifts the energies of the allowed states compared with the free particle, V(R) = 0, case. This results in a small change in the value of the partition function, which is largely independent of the value of L. Since the partition function is proportional to L, the difference between the partition function for $E > 0$ states using $V_d(R)$ and

the free particle partition function, Eq. (12), becomes negligible at large L, justifying the use of Eq. (12) in this work.

The equilibrium constant for the dimerization reaction, Eq. (13), is given by[55]

$$K_{eq} = [AB_1AB_2]/[AB_1][AB_2]$$

$$= (q_d/V)/[(q_1/V)(q_2/V)] \quad (15)$$

This gives $K_{eq} = Vq_d/q_m$. While Eqs. (13) and (15) are written for the AB-AB alignment, the analysis applies for the AB-BA and BA-AB alignments as well. A value for V of $2.5x10^4$ Bohr radii (~$1.32x10^3$ nm), which was used in all calculations, was found to be large enough to justify the use of the classical partition function, Eq. (12), for the translations. The partition functions q_d, q_1, and q_2 are proportional to the value chosen for V due to the form of the translational partition function, Eq, (12). On the other hand, the q/V factors in Eq. (15) are independent of V, as is K_{eq}. The box length does not enter into the calculations other than as the volume factor in the translational partition functions and in the q/V factors in Eq. (15).[57]

III. Results

Calculations were performed for five different sets of potential energy parameters for the one-dimensional AB dimer model. These parameter sets are given in table 1. Five parameter sets are used in the calculations in order to test the sensitivity of the results to the potential model employed. The set of potential energy parameters labeled as set 1 contains the parameters described above with the LJ parameters fit to solubility data[48]. The set 2 parameters use different LJ parameters, which were optimized for DNA bases in water[49]. Using a significantly different set of LJ parameters for comparison provides useful information concerning the robustness of the qualitative findings discussed below. The set 3 parameters are the same as the first set, except μ_0 is multiplied by 1.2. Similarly, the set 4 parameters are the

same as the first set, except μ_1 is now multiplied by 1.2. The set 5 parameters are the same as set 1 except that $\mu_1 = \mu_2 = 0$, which removes the r dependence of the dipoles. Even though the bond length-dependent intermolecular dipolar coupling is turned off in this case, the LJ potentials depend on r_1 and r_2, as can be seen in Eq. (1), and this still results in the vibrations of the two AB molecules being coupled since $\partial^2 V / \partial r_1 \partial r_2 \neq 0$.

Three AB dimer combinations with different isotopic composition for the AB molecules are compared in table 2 for the AB-AB alignment. In the first case, both AB molecules are $^{14}A^{16}B$. In the second case, one molecule is $^{14}A^{16}B$ and the other is $^{15}A^{16}B$, while in the third case, both molecules are $^{15}A^{16}B$. The masses for ^{14}A, ^{15}A, ^{16}B correspond to the isotope masses for ^{14}N, ^{15}N, and ^{16}O, respectively. Each line in table 2 compares the dimer partition functions, q_d, and $K_{eq} = Vq_d/q_m$, for two different AB-AB isotopologues, where V is the box length. One of the dimers is either $^{14}A^{16}B$-$^{14}A^{16}B$ or $^{15}A^{16}B$-$^{15}A^{16}B$ and the other dimer is always $^{14}A^{16}B$-$^{15}A^{16}B$. The monomer partition function, q_m, does not depend on the potential parameters, and its value is provided in the table caption for the three isotopic cases considered. The ratio of the non-covalent dimerization equilibrium constants, Eq. (15), for the different dimers is also given in table 2. The ratio of the K_{eq}'s provides the relative monomer-dimer fractionation of the different isotopic species. All calculations are at T = 150 K. (For comparison, the NO boiling point is 121 K.)

The results from the set 1 potential parameters show that the ratio of dimer-monomer equilibrium constants for the $^{14}A^{16}B$-$^{14}A^{16}B$ case and for the $^{14}A^{16}B$-$^{15}A^{16}B$ case is equal to 0.9563 for the coupled calculation. Since the ratio of these equilibrium constants is less than one, $^{15}A^{16}B$ molecules would have a higher than statistical abundance in the dimer, while $^{14}A^{16}B$ molecules would have a higher than statistical abundance in the monomer form in this system. This change due to the intermolecular coupling of the vibrations is quite large. The variations in

isotopic fractionation in real systems are typically a few tenths of a percent for this ratio. The ratio of the dimer-monomer equilibrium constant from the uncoupled calculation is 1.0053, giving smaller preference for $^{14}A^{16}B$ molecules in the dimer form. Thus, the very significant preferential placement of the ^{15}A into the dimer when the vibrations of the two molecules are coupled is not reproduced in the calculations with uncoupled vibrations. This shows that, in this model system, the coupling of the vibrations of the two AB molecules, and the relaxation of the bond length to the minimum of $V(R, r_1, r_2)$, has a significant effect on the isotopic fractionation between the monomer and the dimer. On the other hand, the ratio of the equilibrium constants for the $^{14}A^{16}B$ - $^{15}A^{16}B$, $^{15}A^{16}B$ - $^{15}A^{16}B$ comparison are nearly the same for the coupled and uncoupled calculations, yielding essentially the same fractionation for the two calculations.

It should be noted that, in the $^{14}A^{16}B$-$^{15}A^{16}B$ and $^{15}A^{16}B$-$^{15}A^{16}B$ systems, the dimer partition functions and K_{eq} are about 0.3%-0.4% different between coupled and uncoupled calculations, compared to roughly a 5.5% difference for the $^{14}A^{16}B$-$^{14}A^{16}B$ system. The coupled K_{eq} is 3.802 and uncoupled K_{eq} is 4.011 for $^{15}A^{16}B$-$^{15}A^{16}B$ system. The corresponding numbers are 3.976 and 3.990 for the $^{14}A^{16}B$-$^{15}A^{16}B$ system. A higher $K_{eq} = Vq_d/q_m$ corresponds to more of the AB in the dimer form. Thus, these differences in q_d correspond to a change in the fraction of AB molecules in dimer form when the dipolar and LJ intermolecular vibrational couplings are accounted for.

The large 5.5% reduction in the ratio of the equilibrium constants when going from the uncoupled to the coupled calculations for the $^{14}A^{16}B$-$^{14}A^{16}B$ system results primarily from the fact that there is one less bound dimer state in the coupled calculations than in the uncoupled calculations. When the center-of-mass distance between two AB molecules is large, the dipole-dipole interaction dominates and decays with a relatively slow R^{-3} dependence. This slow asymptotic approach to zero results in the highest energy bound states lying very close to the E =

0 dissociation limit. As a consequence, a relatively small change in $V_d(R)$ can result in a change in the number of bound states for the dimer.

The potential parameter set 2, in which different LJ parameters are used, and the potential parameter set 4, in which the μ_1 dipole parameter is increased by 20%, provide the same qualitative results as parameter set 1. The partition function and K_{eq} values obtained from the coupled and uncoupled calculations for the $^{14}A^{16}B$-$^{15}A^{16}B$ dimer and $^{15}A^{16}B$-$^{15}A^{16}B$ dimer differ by about 0.3%-0.4%, and the number of bound states for the $^{14}A^{16}B$-$^{14}A^{16}B$ dimer differs by one in the two calculations. While the parameter set 4 results differ from the parameter set 1 results only very slightly, it was found that, if the value of μ_1 was increased to 1.3 times its parameter set 1 value, then the number of bound states for the case 2 coupled calculations changed from 14 to 13. This results in the corresponding partition function changing from 2.818×10^4 for parameter 4 to 2.681×10^4, while K_{eq} changes from 3.975 to 3.781. The ratio of K_{eq}'s changes from 0.9563 to 1.0052 for the case1/case2 system, and it changes from 0.9944 to 1.0452 for the case3/case2 system, demonstrating the sensitivity of the results to the μ_1 parameter.

A change in the number of bound states is not present for parameter set 3, for which the magnitude of the dipole at r_e is increased by 20% compared with the parameter set 1. Since the μ_1 parameter is not increased, this amounts to a smaller fractional increase in the dipole with increasing r, and it is this r-dependent increase in μ that couples the dipoles of the two AB molecules. In this case, there is still an approximately 0.4% difference between coupled and uncoupled partition functions and equilibrium constants. There is also not a change in the number of bound states when using parameter set 5, which neglects the bond length dependence of the dipole moments. In this case, the difference between the coupled and uncoupled partition functions and equilibrium constants shrinks to about 0.25%. While this is smaller than when the dipolar vibrational coupling is included, it is not negligible, which indicates that the LJ

interactions by themselves can induce non-negligible coupling between the vibrations of different molecules. On the other hand, the change in the number of bound dimer states is only seen in the cases in which there is a strong dependence of the molecular dipole on bond length.

The solid line in Fig. 2a shows $V_d(R)$ from the coupled calculations for the $^{14}A^{16}B$-$^{14}A^{16}B$ dimer case when set 1 potential parameters are used. Fig. 2b shows coupled and uncoupled $V_d(R)$ near the minimum for this dimer. The difference between the coupled and uncoupled V_d is larger at small R and approaches zero as R increases, which is to be expected given that the interactions between the molecules are greater when R is small. The difference between the minimum energy bond length for the AB molecule and the bond length for an isolated AB molecule, which we denote as $x_j = r_{j,min} - r_e$, is plotted in Fig. 3 for the coupled $^{14}A^{16}B$-$^{14}A^{16}B$ dimer case using set 1 potential parameters. The position of the potential minimum, R_{mn}, and the value of $V_d(R_{mn})$ are compared for the coupled and uncoupled calculations, all pairs of isotopologues, and all parameter sets for the AB-AB alignment in table 3.

The results from calculations with the AB monomers in the AB-BA and BA-AB alignments are reported in tables 4 and 5, respectively, for parameter sets 1, 2, and 4, which are the sets for which there are changes in the number of bound state in the AB-AB case. The values of R_{rm} and $V_d(R_{mn})$ for these coupled and uncoupled calculations are given in table 3. The $V_d(R)$ for two $^{14}A^{16}B$ molecules and parameter set 1 is also plotted for AB-BA and BA-BA in fig. 2a. In these arrangements the dipole interactions are repulsive. At short and moderate distances the Lennard-Jones attractions are stronger than the dipolar repulsion, and the resulting interactions between the two molecules supports bound dimer states.

R_{mn} shifts to smaller R and $V_d(R_{mn})$ is more negative for AB-BA compared with the AB-AB case. The LJ repulsive R^{-12} dependence is steeper than the R^{-3} dipolar repulsion at small R. R is the distance between the center of mass of the two molecules. It is the B-B LJ repulsion in

AB-BA the largely determines how small R_{mn} gets in this case, while it is a B-A LJ repulsion in AB-AB that determines R_{mn}. Since B is heavier, the center of mass of the molecule is closer to the B atom than the A atom. Furthermore, B has a smaller Lennard-Jones σ parameter than A. This is why R_{mn} for AB-BA is smaller than the R_{mn} for AB-AB. A similar argument explains why R_{mn} for BA-AB is larger than for AB-AB. A smaller R_{mn} results in stronger LJ attractions for three pairs of atoms that are not the closest pair, and this in turn produces a lower $V_d(R_{mn})$ for AB-BA and a higher $V_d(R_{mn})$ for AB-BA than for AB-AB.

The attractive R^{-6} LJ potential decays at large R faster than the repulsive the dipole interaction. Therefore, $V_d(R)$ crosses zero at some large R and becomes slightly positive before decaying to zero with the R^{-3} dipolar dependence. Thus, the bound state $V_d(R)$ well does not have the slow - $2\mu(r_1)\mu(r_2)/R^3$ dependence at large R that resulted in the AB-AB dimer having states very close to E = 0. As such, it might be expected that dimers in the AB-BA and BA-AB arrangement will be less likely to have a change in the number of bound states when comparing the coupled and uncoupled calculations. As expected, the cases that had changes in the number of bound states in the AB-AB alignment do not show these changes in the AB-BA and BA-AB alignments. However, the number of bound states does change when comparing the coupled and uncoupled calculation for parameter set 2 with two $^{15}A^{16}B$ molecules.

Table 6 provides the partition function when the contributions of AB-AB, BA-BA, AB-BA, BA-AB orientations of two AB molecules are summed. (The partition function for BA-BA is the same as for AB-AB.) Since the monomer partition functions are independent of the orientation, they are simply four times the monomer partition functions for any of the four alignments. The equilibrium constants derived from these summed partition function and their ratio are also provided in table 6.

The $V_d(R_{mn})$ for the coupled and uncoupled calculations differs by about 1.2 K for the AB-AB case, except when parameter set 5 is used, in which case this difference is approximately 0.8 K. This shift in V_{min} results, for some cases, in a change in the number of dimer bound states when comparing the coupled and uncoupled calculations. Even in the cases where the number of bound dimer states does not change, the approximately 1 K change seen in V_{min} produces a comparable change in the energies of the lower energy bound states. In turn, this produces the roughly 0.3%-0.4% change in the dimer partition function when comparing the coupled and uncoupled dimer partition functions in table 2 for any pair of isotopologues and potential parameter sets 1 through 4 for which the number of bound states is the same for the coupled and uncoupled calculation. The change in q_d decreases to about 0.25% for parameter set 5, for which the bond length dependence of the AB dipole moment is ignored and the change is V_{min} is somewhat smaller.

The differences in $V_d(R_{mn})$ for the coupled and uncoupled calculations are about 0.6K, 0.3K and 0.4K for the AB-BA arrangement and parameter sets 1, 2, and 4, respectively. The corresponding differences for the BA-AB arrangement are 0.4K, 0.2K, and 0.3K. As seen in fig. 2a, the $V_d(R_{mn})$ values are lower and occur at shorter R_{mn} for the AB-BA case than for the AB-AB arrangement, and they are higher and occur at longer R_{mn} for the BA-BA case. The smaller differences between the coupled and uncoupled calculations in the AB-BA and BA-AB calculations are reflected in the small differences in the corresponding K_{eq} values. When the contributions from the four possible orientations on the monomer are summed, there are changes in the number of bound states when comparing the coupled and uncoupled calculations in most cases. The percentage change in the partition function for the coupled and uncoupled calculation in cases for which there is a difference in the number of bound state for the two calculations is less when all four orientations are summed. For instance, the case 1 partition function for

parameter set 1 is about 5.5% higher in table 2 for the uncoupled partition function compared with the coupled partition function, while this change is about 3% in table 6. This 3% change is still very large compared with the few tenths of a percent size of relative fractionation changes typically observed in experimental systems.

IV. Discussion

The calculations in this work show that the mass dependence in the intermolecular interaction, which results from the coupling of the vibrations of the two AB molecules, can have a significant effect on the isotopic fractionation between the dimer and the non-dimerized AB system. This shift in fractionation occurs because the isotope-dependent dipole-dipole and LJ coupling of the vibrations of the two AB molecules results in a change in the R-dependent potential energy between the molecules. This leads to a change in the energy of the dimer bound states, which in turn alters the dimer partition function, but not the partition function for the two AB monomer system. Since the ratio of these two partition functions provides the equilibrium constant for the dimer-monomer equilibrium, a different equilibrium concentration of dimers is predicted when the dipolar coupling is included compared to when it is ignored. The dependence of the dimer potential on the isotopic composition of the AB molecules can also result in a change in the number of AB dimer bound states when the dipole-dipole induced vibrational coupling is included in the calculation. This has an even greater impact on the dimer partition function than the change in $V_d(R)$ alone.

In cases where there is no change in the number of bound dimer states, the isotopic fractionation between the dimer and the monomer species changes less when going from the uncoupled to coupled calculations. While the dimerization equilibrium constants from the coupled and uncoupled calculations differ, this difference largely cancels when the ratio of the $^{14}A^{16}B$, $^{15}A^{16}B$ and $^{15}A^{16}B$, $^{15}A^{16}B$ equilibrium constants is taken, resulting in nearly the same

isotopic monomer-dimer fractionation. However, there is still a change in the predicted dimer concentration in these two systems due to the difference in the uncoupled and coupled equilibrium constants. On the other hand, in the cases in which the number of bound dimer states changes when going from the uncoupled to the coupled calculations, the changes in the dimer partition functions no longer cancel. In this case, the fractionation of the A isotopes between the dimers and the monomers predicted by the uncoupled calculation differs significantly from that predicted by the coupled calculation.

While these calculations have been performed for a simplified one-dimensional co-linear model, the results obtained show that the intermolecular coupling of vibrations in different molecular isotopologues can have an impact on the fractionation of various isotopes in physical and chemical processes. In higher dimensional systems, one would expect that the density of states would increase faster with energy than in a one dimensional system. The changes in the potential energy would still shift the state energies, as it did in this work. Since these shifts should be largest for the lowest energy states, the resulting changes in the partition functions may not be as significant in a many dimensional case as they are in the simple case considered here. Nonetheless, a change in the potential near its minimum of around 1 K, as seen in this work, should have a non-negligible effect on the partition function for systems at room temperature and below. Furthermore, if the density of states increases faster with increasing energy for higher dimensional systems, as expected, then a higher fraction of the bound states would have energies very close to E = 0, and the changes in the potential could more easily produce changes in the number of bound states. If this is the case, the inclusion of the dipolar induced intermolecular vibrational coupling should have a significant impact on isotope fractionation predictions.

References

[1] H. C. Urey, J. Chem. Soc. 562 (1947).

[2] J. Bigeleisen and M. G. Mayer, J. Chem. Phys. **15**, 261 (1947).

[3] M. Wolfsberg, Annu. Rev. Phys. Chem. **20**, 449 (1969).

[4] G. Jancso, L. P. N. Rebelo, W. A. Van Hook, Chem. Rev. **93**, 2645 (1993).

[5] G. Jancso, Radiochemistry and Nuclear Chemistry, Vol 1 of Encyclopedia of Life Support Systems, UNESCO-EOLSS, 2009.

[6] P Baertschi, W. Kuhn, H. Kuhn, Nature **171**, 1018 (1953).

[7] P. M. Grootes, W. G. Mook, J. C. Vogel, Z. Phys. **221**, 257 (1969).

[8] T. Rahn, J. M. Eiler, Geochim. Cosmochim Acta **65**(5), 839 (2001).

[9] N. Moussa, N. Naulet, M. L. Martin, G. J. Martin, J. Phys. Chem. **94**, 8303 (1990).

[10] S. R. Poulson, J. I. Drever, Environ. Sci. Technol. **33**, 3689 (1999).

[11] M. Balabane, R. Letolle, Chem. Geol. **52**, 391 (1985).

[12] J. M. Eiler, P. Cartingny, A. E. Hofmann, A. Piasecki, Geochim. Cosmochim. Acta **107**, 205 (2013).

[13] N. Estrade, J. Carignan, J. E. Sonke, O. F. X. Donard, Geochim. Cosmochim. Acta **73**, 2693 (2009).

[14] S. Ghosh, E. A. Schauble, G. L. Couloume, J. L. Blum, B. A. Bergquist, Chem. Geol. **336**, 5 (2013).

[15] T. Fujii, F. Moynier, P. Telouk, F. Albarede, Chem. Geol. **267**, 139 (2009).

[16] T. Fujii, F. Moynier, P. Telouk, F. Albarede, Chem. Geol. **267**, 157 (2009).

[17] K. Nishizawa, K. Nakamura, T. Yamamoto, T. Masuda, Solvent Extr. Ion Exch. **11**, 389 (1993).

[18] K. Nishizawa, K. Nakamura, T. Yamamoto, T. Masuda, Solvent Extr. Ion Exch. **12**, 1073 (1993).

[19] K. Nishizawa, T. Satoyama, T. Miki, T. Yamamoto, M. Hosoe, J. Nucl. Sci. Tehnol. **32** (12), 1230 (1995).

[20] K. L. Casciotti, Geochim. Cosmochim. Acta **73**, 2061 (2009).

[21] M. H. Thiemens, S. Chakraborty, G. Dominguez, Annu. Rev. Phys. Chem. **63**, 155 (2012).

[22] M. H. Thiemens, Annu. Re. Earth Planet. Sci. **34**, 217 (2006).

[23] M. H. Thiemens, J. E. Heidenreich III, Science **219**, 1073 (1983).

[24] J. Yang, S. Epstein, Geochim. Cosmochem. Acta **51**, 2011 (1987).

[25] R. A. Marcus, Proc. Natl. Acad. Sci. USA **110**(44), 19023 (2013).

[26] A. L. Buchachemko, J. Phys. Chem. B **117**, 2231 (2013).

[27] S. Kopf, O. Shuhei, Geochim. Cosmochim. Acta **85**, 160 (2012).

[28] J. R. Lyons, E. D. Young, Nature **435**, 317 (2005).

[29] M. C. Liang, A. N. Heays, B. R. Lewis, S. T. Gibson, Y. L Yung, Astrophys. J. Lett. **664**, L115 (2007).

[30] G. Briani, M. Gounelle, Y. Marrocchi, S. Mostefaoui, H. Leroux, E. Quirico, A. Melbom, Proc. Natl. Acad. Sci. USA **106**, 10522 (2009).

[31] Q. Lui, J. A. Tossell, Y. Liu, Geochim. Cosmochim. Acta **74**, 6965 (2010).

[32] J. Bigeleisen, J. Am. Chem. Socs. **118**, 3676(1996).

[33] J. Bigeleisen, Proc. Natl. Acad. Sci. USA **95**, 4808 (1998).

[34] M. V. Ivanov, D. Babikov, Proc. Natl. Acad. Sci. USA **110** (44), 17708 (2013).

[35] T. E. Larson and D. O. Breecker (2014) Chem. Geol. **370**, 58 (2014).

[36] M. F. Herman, R. P. Currier, and S. M. Clegg, Chem. Phys. Lett. **639**, 266 (2015).

[37] E. Balan, P. Cartigny, M. Blanchard, D. Cabaret, M. Lazzeri, and F. Mauri, Earth Planet. Sci. Lett. **284**, 88 (2009).

[38] W. T. Rawlins, J. C. Person, M. E. Fraser, S. M. Miller, and W. A. M. Blumberg, J. Chem. Phys. **109**, 3409 (1998).

[39] S. G. Kukolich, J. Am. Chem. Soc. **104**, 4715 (1982).

[40] J. A. Barnes, T. E. Gough, J. Chem. Phys. **86**, 6012 (1987).

[41] R. W. Randall, A. J. Cliffe, B. J. Howard, A. R. W. McKellar, Molecular Physics **79**, 1113 (1993).

[42] M. J. Weida, J. M. Sperhac, and D. J. Nesbitt, J. Chem. Phys. **103**, 7685 (1995).

[43] D. Hou, T.-T. Ma, X.-L. Zhang, and H. Li, J. Chem. Phys. **144,** 014301 (2016).

[44] T. Zimmermann and J. Vanicek, J. Chem. Phys. **131**, 024111 (2009).

[45] T. E. Markland and B. J. Berne, Proc. Natl. Acad. Sci. USA **109**, 7988 (2012).

[46] J. Liu, R. S, Andino, C. M. Miller, X. Chen, D. M. Wilkins, M. Ceriotti, and D. E. Manolopoulos, J. Phys. Chem. C. **117**, 2944, (2013).

[47] G. Romanelli, M. Ceriotti, D. E. Manolopoulos, C. Pantalei, R. Senesi, and C. Andreani, J. Phys. Chem. Lett. **4**, 3251 (2013).

[48] L. Wang, M. Ceriotti, and T. E. Markland, J. Chem. Phys. **141**, 104502 (2014).

[49] E. Wilhelm and R. Battino, J. Chem. Phys. **55**, 4012 (1971).

[50] M. Monajjemi, S. Ketabi, M. H. Zadeh, and A. Amiri, Biochem. (Moscow) **71** (supplement 1), S1 (2006).

[51] Computational Chemistry Comparison and Benchmark DataBase, Release 7b, National Institute of Standards and Technology (USA), (2015).

[52] Since the two AB molecules are taken to be in their vibrational ground states, the difference between the zero-th order vibrational energy, the second order perturbative vibrational energy based on a fourth order expansion of the vibrational potential, and the Morse vibrational ground state energy should be small. To check this, coupled and uncoupled calculations using the zero-

th order vibrational energies were compared with corresponding calculations using the second order perturbation vibrational energies. It was found that the difference in the energies from the two calculations had a negligible effect on the partition functions evaluated using these energies, indicating that the 2nd order perturbation theory results are well converged.

[53] M. S. Child, *Semiclassical Mechanics with Molecular Applications*, Oxford University Press, New York, 1991.

[54] For completeness, there should be Boltzmann 1/n! factors multiplying the partition functions to account for identical particles. These factors are not explicitly included in this work, since they cancel when the ratio of partition functions are formed.

[55] D. A. McQuarrie, "Statistical Mechanics", University Science Books, Mill Valley, CA, 2000.

[56] Since there is a hard wall at the right side of these calculation, the semiclassical quantization condition is $W(E)/\hbar = (n + 3/4)\pi$ instead of that given in Eq. (9).

[57] While the partition functions depend on the value chosen for the box length V, they are dimensionless quantities. As such they are independent of the units used for V. On the other hand, while K_{eq} is independent on the value of V, it has units of volume (i.e., length) and depends on the unit chosen for length.

Table 1. The potential energy parameters employed in the calculations. Energies are in Kelvin, and lengths are in angstroms (10^{-10}m). The dipole parameters are in debye and angstroms. Calculations are performed for five sets of potential parameters.

Set 1: $\varepsilon_B = 1.181 \times 10^2$, $\varepsilon_A = 0.950 \times 10^2$, $\sigma_B = 3.46$, $\sigma_A = 3.70$ (Gas solubility data)[48], $\mu_0 = -0.1681$, $\mu_1 = 2.345$, $\mu_2 = -1.26$[37], $D_e = 9.257 \times 10^4$, $\alpha = 0.6995$, $r_e = 1.172$[50].

Set 2: $\varepsilon_B = 1.058 \times 10^2$ $\varepsilon_A = 0.856 \times 10^2$, $\sigma_B = 2.96$, $\sigma_A = 3.25$ (DNA bases in water data)[49] All other parameters are the same as set 1.

Set 3: μ_0 is 1.2 times the μ_0 for set 1. All other parameters are the same as set 1.

Set 4: μ_1 is 1.2 times the μ_1 for set 1. All other parameters are the same as set 1.

Set 5: $\mu_1 = 0$ and $\mu_2 = 0$. All other parameters are the same as set 1.

Table 2. Result from AB-AB calculations with different isotopic compositions at T = 150K. Case 1 has two $^{14}A^{16}B$ molecules. Case 2 has one $^{14}A^{16}B$ molecule and one $^{15}A^{16}B$ molecule. Case 3 has two $^{15}A^{16}B$ molecules. The n_{bnd} values given in each line are the number of bound dimer states for the two cases, labelled i and j, compared in that line. The molecular calculation is either coupled (cpl) or uncoupled (unc) as indicated. The partition function for the monomer systems, Eq. (14), is 9.227×10^9 for case 1, 9.379×10^9 for case 2, and 9.534×10^9 for case 3. The K_{eq} are in angstroms (10^{-10} m).

Potential parameter set 1:

case i	case j	$n_{bnd,i}$	$n_{bnd,j}$	type	q_{di}	q_{dj}	$K_{eq,i}$	$K_{eq,j}$	$K_{eq,i}/K_{eq,j}$
1	2	13	14	cpl	2.652×10^6	2.819×10^6	3.802	3.976	0.9563
1	2	14	14	unc	2.798×10^6	2.829×10^6	4.011	3.990	1.0053
3	2	14	14	cpl	2.849×10^6	2.819×10^6	3.953	3.976	0.9944
3	2	14	14	unc	2.859×10^6	2.829×10^6	3.968	3.990	0.9944

Potential parameter set 2:

case i	case j	$n_{bnd,i}$	$n_{bnd,j}$	type	q_{di}	q_{dj}	$K_{eq,i}$	$K_{eq,j}$	$K_{eq,i}/K_{eq,j}$
1	2	11	12	cpl	2.019×10^6	2.177×10^6	2.894	3.071	0.9425
1	2	12	12	unc	2.162×10^6	2.185×10^6	3.100	3.081	1.0059
3	2	12	12	cpl	2.199×10^6	2.177×10^6	3.052	3.071	0.9937
3	2	12	12	unc	2.207×10^6	2.185×10^6	3.062	3.081	0.9937

Potential parameter set 3:

case i	case j	$n_{bnd,i}$	$n_{bnd,j}$	type	q_{di}	q_{dj}	$K_{eq,i}$	$K_{eq,j}$	$K_{eq,i}/K_{eq,j}$
1	2	14	14	cpl	2.801×10^6	2.833×10^6	4.017	3.996	1.0052
1	2	14	14	unc	2.812×10^6	2.844×10^6	4.032	4.011	1.0053
3	2	14	14	cpl	2.863×10^6	2.833×10^6	3.973	3.996	0.9943
3	2	14	14	unc	2.874×10^6	2.844×10^6	3.989	4.011	0.9943

Potential parameter set 4:

case i	case j	$n_{bnd,i}$	$n_{bnd,j}$	type	q_{di}	q_{dj}	$K_{eq,i}$	$K_{eq,j}$	$K_{eq,i}/K_{eq,j}$
1	2	13	14	cpl	2.651×10^6	2.818×10^6	3.801	3.975	0.9563
1	2	14	14	unc	2.798×10^6	2.829×10^6	4.011	3.990	1.0053
3	2	14	14	cpl	2.848×10^6	2.818×10^6	3.952	3.975	0.9944
3	2	14	14	unc	2.859×10^6	2.829×10^6	3.968	3.990	0.9944

Potential parameter set 5:

case i	case j	$n_{bnd,i}$	$n_{bnd,j}$	type	q_{di}	q_{dj}	$K_{eq,i}$	$K_{eq,j}$	$K_{eq,i}/K_{eq,j}$
1	2	14	14	cpl	2.791×10^6	2.822×10^6	4.002	3.981	1.0053
1	2	14	14	unc	2.798×10^6	2.829×10^6	4.011	3.990	1.0053
3	2	14	14	cpl	2.852×10^6	2.822×10^6	3.958	3.981	0.9943
3	2	14	14	unc	2.859×10^6	2.829×10^6	3.968	3.990	0.9944

Table 3. The minimum in $V_d(r)$ and its position, R_{mn}. Case 1 has two $^{14}A^{16}B$ molecules. Case 2 has one $^{14}A^{16}B$ molecule and one $^{15}A^{16}B$ molecule. Case 3 has two $^{15}A^{16}B$ molecules. The calculation type is either coupled (cpl) or uncoupled (unc). The potential parameters for the five sets are given in table 1. V_d is given in Kelvin and R_{mn} is in angstroms (10^{-10}m).

AB-AB		Set 1		Set 2		Set 3		Set 4		Set 5	
Case	Type	R_{mn}	$V_d(R_{mn})$	R_{mn}	$V_d(R_{mn})$	R_{mn}	$V_d(R_{mn})$	R_{mn}	$V_d(R_{mn})$	R_{mn}	$V_d(R_{mn})$
1	cpl	5.02	-213.08	4.52	-175.00	5.02	-214.44	5.02	-213.00	5.02	-213.42
1	unc	5.01	-214.25	4.52	-176.21	5.01	-215.68	5.01	-214.25	5.01	-214.25
2	cpl	5.00	-213.14	4.50	-175.08	5.00	-214.51	5.00	-213.06	5.00	-213.47
2	unc	4.99	-214.29	4.50	-176.27	4.99	-215.74	4.99	-214.29	4.99	-214.29
3	cpl	5.02	-213.10	4.52	-175.03	5.02	-214.46	5.02	-213.02	5.02	-213.43
3	unc	5.01	-214.25	4.52	-176.21	5.01	-215.68	5.01	-214.25	5.01	-214.25

AB-BA		Set 1		Set 2		Set 4	
Case	Type	R_{mn}	$V_d(R_{mn})$	R_{mn}	$V_d(R_{mn})$	R_{mn}	$V_d(R_{mn})$
1	cpl	4.81	-235.61	4.29	-194.69	4.81	-235.70
1	unc	4.81	-236.12	4.28	-194.99	4.81	-236.12
2	cpl	4.83	-235.64	4.31	-194.75	4.83	-235.73
2	unc	4.83	-236.17	4.30	-195.06	4.83	-236.17
3	cpl	4.85	-235.68	4.33	-194.80	4.85	-235.76
3	unc	4.85	-236.21	4.32	-195.13	4.85	-236.21

BA-AB		Set 1		Set 2		Set 4	
Case	Type	R_{mn}	$V_d(R_{mn})$	R_{mn}	$V_d(R_{mn})$	R_{mn}	$V_d(R_{mn})$
1	cpl	5.23	-183.04	4.77	-143.94	5.23	-181.84
1	unc	5.22	-183.46	4.76	-144.14	5.22	-182.19
2	cpl	5.21	-183.02	4.75	-143.91	5.21	-181.81
2	unc	5.29	-183.43	4.74	-144.09	5.20	-182.15
3	cpl	5.19	-183.01	4.73	-143.88	5.19	-181.78
3	unc	5.18	-183.39	4.72	-144.05	5.18	-182.10

Table 4. Results from AB-BA calculations with different isotopic compositions at T = 150K. Case 1 has two $^{14}A^{16}B$ molecules. Case 2 has one $^{14}A^{16}B$ molecule and one $^{15}A^{16}B$ molecule. Case 3 has two $^{15}A^{16}B$ molecules. The n_{bnd} values given in each line are the number of bound dimer states for the two cases, labelled i and j, compared in that line. The molecular calculation is either coupled (cpl) or uncoupled (unc) as indicated. The partition function for the monomer systems, Eq. (14), is is 9.227×10^9 for case 1, 9.379×10^9 for case 2, and 9.534×10^9 for case 3. The K_{eq} are in angstroms (10^{-10} m).

Potential parameter set 1:

case i	case j	$n_{bnd,i}$	$n_{bnd,j}$	type	q_{di}	q_{dj}	$K_{eq,i}$	$K_{eq,j}$	$K_{eq,i}/K_{eq,j}$
1	2	11	11	cpl	2.541×10^6	2.572×10^6	3.644	3.627	1.0046
1	2	11	11	unc	2.545×10^6	2.575×10^6	3.649	3.633	1.0045
3	2	11	11	cpl	2.602×10^6	2.572×10^6	3.611	3.627	0.9954
3	2	11	11	unc	2.606×10^6	2.576×10^6	3.616	3.633	0.9954

Potential parameter set 2:

case i	case j	$n_{bnd,i}$	$n_{bnd,j}$	type	q_{di}	q_{dj}	$K_{eq,i}$	$K_{eq,j}$	$K_{eq,i}/K_{eq,j}$
1	2	8	8	cpl	1.694×10^6	1.713×10^6	2.428	2.416	1.0049
1	2	8	8	unc	1.695×10^6	1.714×10^6	2.430	2.418	1.0048
3	2	9	8	cpl	1.871×10^6	1.713×10^6	2.596	2.416	1.0744
3	2	8	8	unc	1.734×10^6	1.714×10^6	2.406	2.418	0.9951

Potential parameter set 4:

case i	case j	$n_{bnd,i}$	$n_{bnd,j}$	type	q_{di}	q_{dj}	$K_{eq,i}$	$K_{eq,j}$	$K_{eq,i}/K_{eq,j}$
1	2	11	11	cpl	2.542×10^6	2.573×10^6	3.645	3.629	1.0046
1	2	11	11	unc	2.545×10^6	2.576×10^6	3.649	3.633	1.0045
3	2	11	11	cpl	2.603×10^6	2.573×10^6	3.612	3.629	0.9954
3	2	11	11	unc	2.606×10^6	2.576×10^6	3.616	3.633	0.9954

Table 5. Results from BA-AB calculations with different isotopic compositions at T = 150K. Case 1 has two $^{14}A^{16}B$ molecules. Case 2 has one $^{14}A^{16}B$ molecule and one $^{15}A^{16}B$ molecule. Case 3 has two $^{15}A^{16}B$ molecules. The n_{bnd} values given in each line are the number of bound dimer states for the two cases, labelled i and j, compared in that line. The molecular calculation is either coupled (cpl) or uncoupled (unc) as indicated. The partition function for the monomer systems, Eq. (14), is 9.227×10^9 for case 1, 9.379×10^9 for case 2, and 9.534×10^9 for case 3. The K_{eq} are in angstroms (10^{-10} m).

Potential parameter set 1:

case i	case j	$n_{bnd,i}$	$n_{bnd,j}$	type	q_{di}	q_{dj}	$K_{eq,i}$	$K_{eq,j}$	$K_{eq,i}/K_{eq,j}$
1	2	10	10	cpl	2.025×10^6	2.047×10^6	2.903	2.888	1.0055
1	2	10	10	unc	2.027×10^6	2.049×10^6	2.907	2.891	1.0055
3	2	10	10	cpl	2.069×10^6	2.047×10^6	2.872	2.888	0.9945
3	2	10	10	unc	2.072×10^6	2.049×10^6	2.875	2.891	0.9944

Potential parameter set 2:

case i	case j	$n_{bnd,i}$	$n_{bnd,j}$	type	q_{di}	q_{dj}	$K_{eq,i}$	$K_{eq,j}$	$K_{eq,i}/K_{eq,j}$
1	2	8	8	cpl	1.457×10^6	1.472×10^6	2.089	2.077	1.0061
1	2	8	8	unc	1.458×10^6	1.472×10^6	2.090	2.077	1.0062
3	2	8	8	cpl	1.487×10^6	1.472×10^6	2.064	2.077	0.9938
3	2	8	8	unc	1.487×10^6	1.472×10^6	2.064	2.077	0.9938

Potential parameter set 4:

case i	case j	$n_{bnd,i}$	$n_{bnd,j}$	type	q_{di}	q_{dj}	$K_{eq,i}$	$K_{eq,j}$	$K_{eq,i}/K_{eq,j}$
1	2	10	10	cpl	2.026×10^6	2.048×10^6	2.904	2.888	1.0055
1	2	10	10	unc	2.027×10^6	2.049×10^6	2.907	2.891	1.0055
3	2	10	10	cpl	2.070×10^6	2.048×10^6	2.873	2.888	0.9945
3	2	10	10	unc	2.072×10^6	2.049×10^6	2.875	2.891	0.9944

Table 6. Results from dimer calculations with different isotopic compositions at T = 150K. The partitions functions are the sum of all four orientations of the two dimers, i.e., AB or BA for each dimer. Case 1 has two $^{14}A^{16}B$ molecules. Case 2 has one $^{14}A^{16}B$ molecule and one $^{15}A^{16}B$ molecule. Case 3 has two $^{15}A^{16}B$ molecules. The n_{bnd} values given in each line are the number of bound dimer states for the two cases, labelled i and j, compared in that line. The molecular calculation is either coupled (cpl) or uncoupled (unc) as indicated. The partition function for the monomer systems, Eq. (14), is 3.691×10^{10} for case 1, 3.752×10^{10} for case 2, and 3.813×10^{10} for case 3. The K_{eq} are in angstroms (10^{10}m).

Potential parameter set 1:

case i	case j	$n_{bnd,i}$	$n_{bnd,j}$	type	q_{di}	q_{dj}	$K_{eq,i}$	$K_{eq,j}$	$K_{eq,i}/K_{eq,j}$
1	2	47	49	cpl	1.974×10^7	2.051×10^7	3.538	3.617	0.9782
1	2	49	49	unc	2.034×10^7	2.057×10^7	3.645	3.626	1.0052
3	2	49	49	cpl	2.074×10^7	2.051×10^7	3.597	3.617	0.9946
3	2	49	49	unc	2.079×10^7	2.057×10^7	3.607	3.626	0.9946

Potential parameter set 2:

case i	case j	$n_{bnd,i}$	$n_{bnd,j}$	type	q_{di}	q_{dj}	$K_{eq,i}$	$K_{eq,j}$	$K_{eq,i}/K_{eq,j}$
1	2	38	40	cpl	1.438×10^7	1.508×10^7	2.576	2.659	0.9691
1	2	40	40	unc	1.495×10^7	1.511×10^7	2.680	2.664	1.0057
3	2	42	40	cpl	1.512×10^7	1.508×10^7	2.691	2.659	1.0121
3	2	40	40	unc	1.527×10^7	1.511×10^7	2.649	2.664	0.9940

Potential parameter set 4:

case i	case j	$n_{bnd,i}$	$n_{bnd,j}$	type	q_{di}	q_{dj}	$K_{eq,i}$	$K_{eq,j}$	$K_{eq,i}/K_{eq,j}$
1	2	49	49	cpl	1.974×10^7	2.051×10^7	3.538	3.617	0.9782
1	2	49	49	unc	2.034×10^7	2.057×10^7	3.645	3.626	1.0052
3	2	49	49	cpl	2.074×10^7	2.051×10^7	3.597	3.617	0.9946
3	2	49	49	unc	2.079×10^7	2.057×10^7	3.607	3.626	0.9946

	AB_1	AB_2
Isotopologue Case 1:	$^{14}A^{16}B$	$^{14}A^{16}B$
Isotopologue Case 2:	$^{14}A^{16}B$	$^{15}A^{16}B$
Isotopologue Case 3:	$^{15}A^{16}B$	$^{15}A^{16}B$

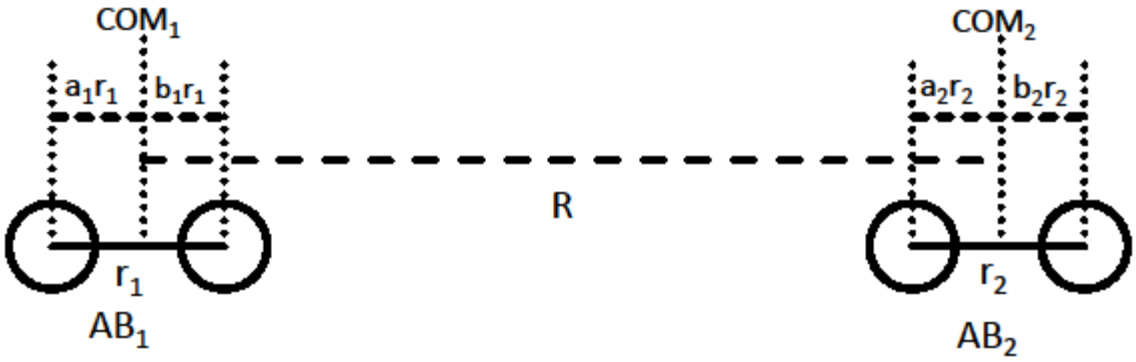

Figure 1. Co-linear AB-AB system. The left circle for each molecule is the A atom and the right circle are the B atoms. R is the distance between the center of mass of AB_1 and the center of mass of AB_2. The bond lengths for the two molecules are r_1 and r_2. The a_jr_j is the distance of the A atom from the center of mass for molecule j (j = 1, 2), and b_jr_j is the distance of the B atom from the center of mass of the molecule.

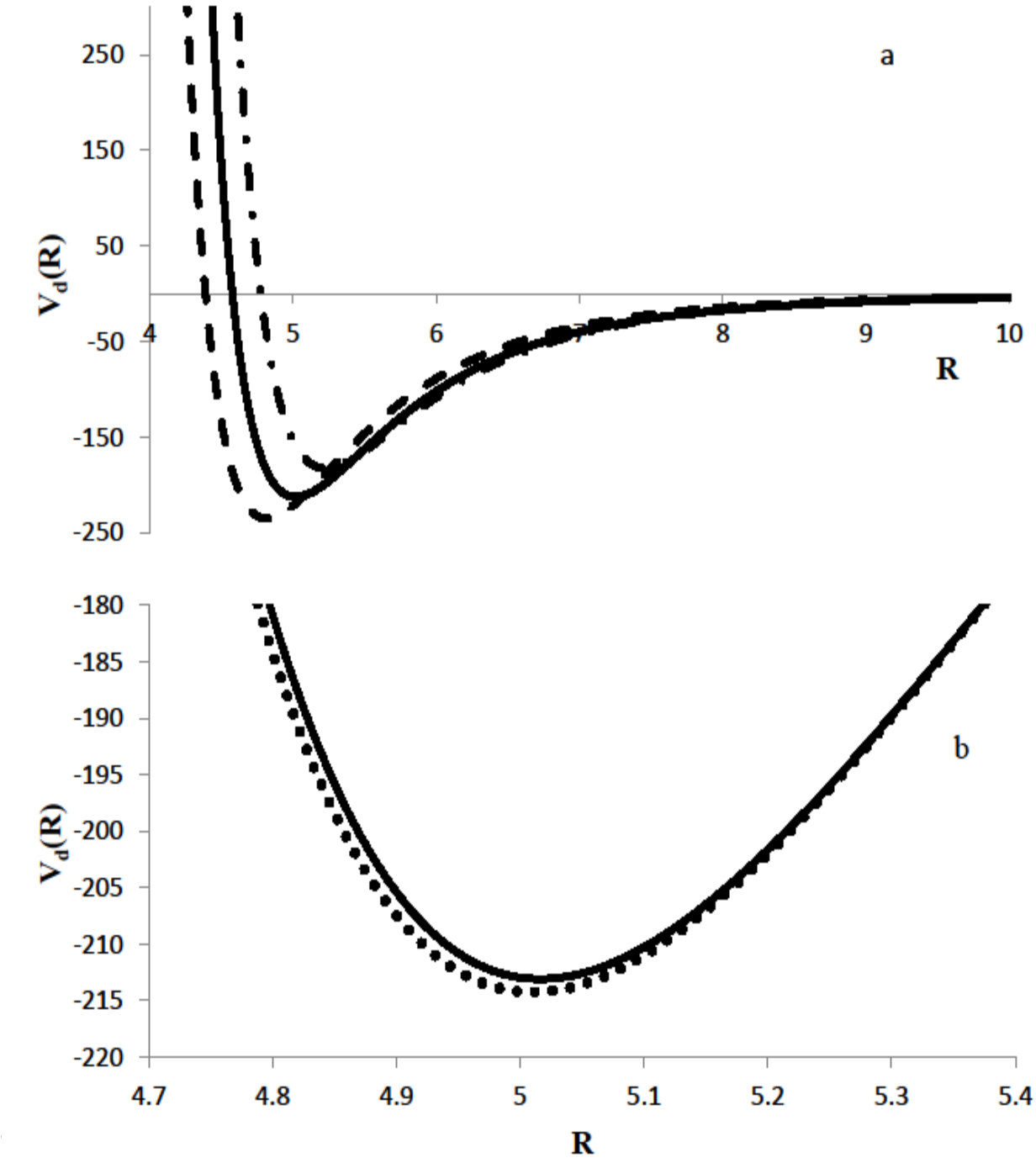

Figure 2. (a) $V_d(R)$ from coupled calculations for AB-AB (solid curve), AB-BA (dashed curve), and BA-AB (dot-dash curve). (b) $V_d(R)$ near minimum for coupled (solid curve) and uncoupled (dotted curve) calculations. Calculations are for the $^{14}A^{16}B$-$^{14}A^{16}B$ system with parameters from set 1. V_d is in Kelvin and R is in angstroms.

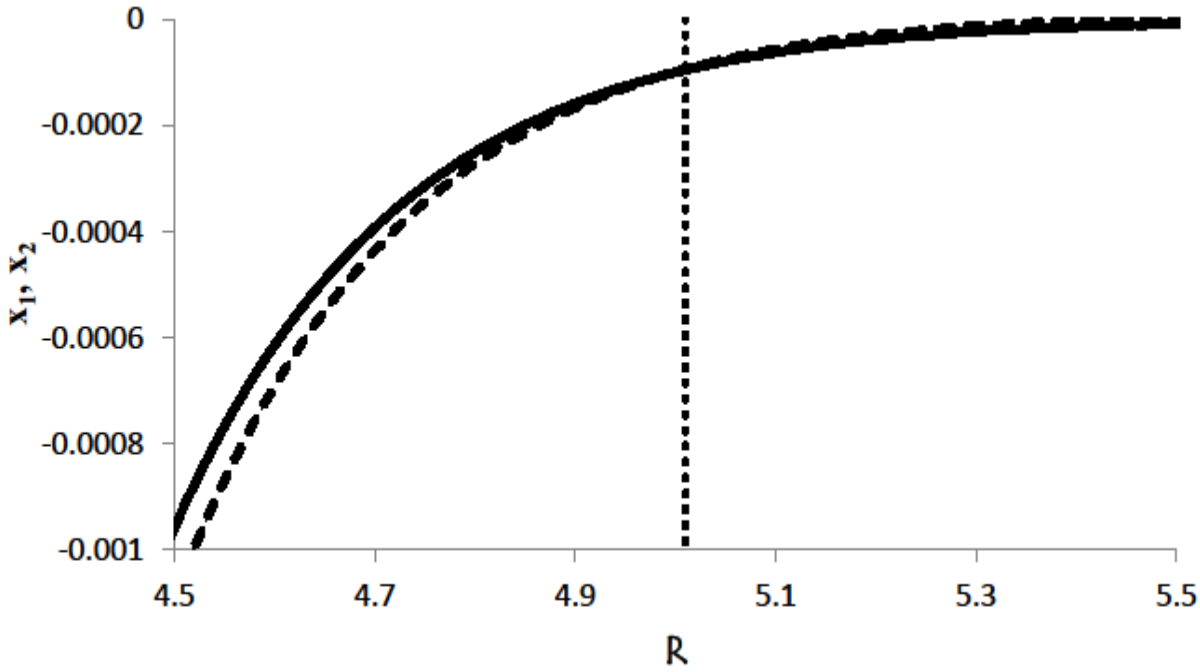

Figure 3. Plot of $x_1 = r_{1,min} - r_e$ (solid curve) and $x_2 = r_{2,min} - r_e$ (dashed curve) as functions of R for the $^{14}A^{16}B$-$^{14}A^{16}B$ case using parameter set 1 for the potential. The dotted line is at R = 5.01, which is the position of the minimum for the coupled $V_d(R)$. The R, x_1, and x_2 values are in angstroms. Since the center of mass of AB is closer to the heavier element (i.e., B), a change in r_2 at fixed R produces a larger change in the short distance between atom B from molecule 1 and atom A from molecule 2 than the same size change in r_1. This asymmetry results in the difference in two curves in the figure.